Nano Energy 79 (2021) 105434

Contents lists available at ScienceDirect

Nano Energy

journal homepage: http://www.elsevier.com/locate/nanoen

Enhancing the filtration efficiency and wearing time of disposable surgical masks using TENG technology

Ruichao Zhang [a], Qi Xu [b], Suo Bai [a], Jun Hai [c], Li Cheng [a], Guoqiang Xu [c], Yong Qin [a,*]

[a] Insitute of Nanoscience and Nanotechnology, School of Physical Science and Technology, Lanzhou University, Lanzhou 730000, China
[b] School of Advanced Materials and Nanotechnology, Xidian University, Xi'an 710071, China
[c] State Key Laboratory of Applied Organic Chemistry Lanzhou University and Key Laboratory of Nonferrous Metal Chemistry and Resources Utilization of Gansu Province, Lanzhou University, Lanzhou 730000, China

ARTICLE INFO

Keywords:
COVID-19
Disposable surgical masks
Filtration
Meltblown nonwoven filter
Triboelectric nanogenerator
Decontamination

ABSTRACT

The COVID-19 pandemic has caused an unprecedented human and health crisis. And the shortage of protective equipment, especially the personal protective disposable surgical masks, has been a great challenge. Here, we developed an effective and simple scheme to prolong the lifetime of disposable surgical masks without changing their current structure, which is beneficial to solve the shortage of personal masks. After electrifying the melt-blown PP filter by the new-developed single-electrode-based sliding triboelectric nanogenerator (TENG) charge replenishment (NGCR) technology, the processed filter is bipolar charged and has a filtration efficiency beyond 95% for the particulate matter (PM) ranging from $PM_{0.3}$ to $PM_{10.0}$. Further, we demonstrate the 80 °C dry heating is an effective decontamination method. This method is compatible with single-electrode-based sliding TENG charge replenishment technology. The 80 °C dry heating and the NGCR technology can make up an effective regeneration procedure for the mask. Even after ten cycles of simulated 4 h wearing process and such regeneration procedure, the filtration efficiency of the disposable surgical masks $PM_{0.3}$ is still higher than 95%.

1. Introduction

The burst of Coronavirus (COVID-19) has brought about a hugely adverse effect on the social and economic framework. It is necessary to prevent its further expansion. Relevant researches show that COVID-19 spreads mainly between humans through direct or indirect contact, respiratory droplets and droplet nuclei generated from coughs, sneezes, or speaks [1–4]. Wearing disposable surgical masks is one effective way to hinder the virus transmission, as the respiratory droplets and droplet nuclei with COVID-19 can be largely removed when they pass through the filter layer of the mask [5,6]. All mechanisms of human oro-nasal activity such as breathing, talking, laughing, coughing and sneezing produce particles within the inhalable range for humans of submicron (< 1 μm) to > 100 μm [7]. As for particulate matter (PM) in submicron region, the filtration efficiency of mechanical filtering mechanisms such as Brownian diffusion, interception, and inertial impaction are insufficient [8–10]. The US Centers for Disease Control and Prevention (CDC) pointed out that as for the particles with sizes of about 0.3 μm, masks based on the mechanical filtering mechanism have the lowest filtration efficiency [11]. Thus, 0.3 μm sized particles can be used to assess the masks' overall filtration efficiency. Because, if the mask has a high filtration efficiency toward 0.3 μm sized particles, then it will have a even higher filtration efficiency toward smaller or larger sized particles. What's more, if the mask has a high filtration efficiency toward 0.3 μm sized particles, it can be used to protect people from respiring inhalable particles carrying COVID-19 in the whole range (with size < 1 μm to $>$ 100 μm). Fortunately, electrostatic attraction can be used, the electrostatic filtration can remove particles with large sizes ranging from nanoparticles with a filtration efficiency beyond 90% [12,13]. However, the charges on the filter layer will gradually dissipate due to the water vapor respiration [14–16]. In practice, the disposable surgical masks generally can continuously and effectively work about 4–8 h depending on the using environment. So, in order to control and prevent the further expansion of COVID-19, a large amount of disposable surgical masks is needed, which brings about huge pressure on disposable surgical masks' production. Therefore, the technologies of developing high performance disposable surgical masks with a long lifetime and more wearing times are greatly needed.

Up to now, there exist some of the works devoting to this issue through the new design of the mask's structure. Zhang reported a self-

* Corresponding author.
E-mail address: qinyong@lzu.edu.cn (Y. Qin).

https://doi.org/10.1016/j.nanoen.2020.105434
Received 18 June 2020; Received in revised form 23 September 2020; Accepted 24 September 2020
Available online 5 October 2020

powered filter, in which an electric field generated by a micro-button lithium cell or silicon-based solar panel across an ionic liquid-polymer is used to remove $PM_{2.5}$ with an efficiency of 93.77% [17]. Besides the conventional batteries, TENG has emerged as a powerful technology with the ability to harvest the ambient mechanical energy and convert them into electricity [18–22]. The output voltage of TENG can be up to several hundred volts and is used to charge the filter or construct electric filed in the filter layer for better $PM_{2.5}$ filtration efficiency [23]. Utilizing the rotating TENG as a power supply, Chen et al. first introduced a self-powered air cleaning system for removing SO_2 and PMs in 2014; [24] Feng and coworkers demonstrated a self-powered filter by combining TENG and photocatalysis technique for removing organic vapor pollutants in the indoor atmosphere [25]. However, no matter using ionic liquid-polymer equipped with an external battery or utilizing TENGs to form a self-powered filter system, either new materials or novel designs are needed. The huge pressure on disposable surgical masks' production can't be relieved as these techniques are not compatible with the current assembly line for disposable surgical masks. In this urgent time, exploring a simple and effective method that can be realized by everyone at home to increase the working lifetime and wearing times of current disposable surgical masks on the market is a possible and viable scheme to solve the extreme shortage of disposable surgical masks.

Here, we demonstrated a regeneration procedure for disposable surgical masks to increase their working lifetime and wearing times. This procedure doesn't need to change the structure or replace the materials of the current disposable surgical masks. This regeneration procedure is composed of an 80 °C dry heating decontamination and a subsequent NGCR technology. Even after ten cycles of such regeneration procedures, the filtration efficiency of the disposable surgical masks towards $PM_{0.3}$ is still higher than 95%, which means the lifetime and wearing times of general disposable surgical masks can be increased at least 10 times compared to their normal situation.

2. Results

2.1. Particulate matter filtration test and performance of the disposable surgical masks

As shown in the inset of Fig. 1a, a disposable surgical mask is composed of 3 layers, which are outer layer, filter layer and the inner layer, respectively. The outer layer is made of hydrophobic non-woven polypropylene (PP), and is used to prevent external moisture in the inhaled air from entering the filter layer. The filter layer is made of meltblown non-woven PP, and is used to capture oil and non-oil particles in the inhaled air. The inner layer is also made of hydrophobic non-woven PP layer and is used to block the accesses of moisture in the exhaled air to the filter layer. The filtration efficiency of the disposable surgical mask is determined by the filter layer, as compared with the inner and outer layer, the non-woven polypropylene is denser as shown in Fig. S1. As shown in Fig. 1b, if the filter is charged by rubbing it with a PTFE film by hand, its filtration efficiency can be improved notably, especially for nanoparticles with a small size. After rubbing, the surface potential of the filter can increase from 1.5 V to 343 V followed by a slow decay with an electrostatic voltmeter (ESVM) (Fig. 1c), which means the improved filtration efficiency can be maintained for a long time. After charged, by testing the filter's filtration efficiency against time (Fig. 1d), it is found that even after 16 h (h) the rubbed filter still shows a higher filtration efficiency of 68% compared with its original efficiency of 45.4% without charging process.

2.2. Meltblown PP filter charging design and working principle

Although charged meltblown PP filter by rubbing the filter with the PTFE film can make the filter charged (Fig. 2a, case I) and enhance its filtration efficiency, the charge in the filter is of one sign (Fig. 2b, case I), the maximum electric field locates just outside the meltblown PP filter, which will not effectively contribute to the filter efficiency [26]. To

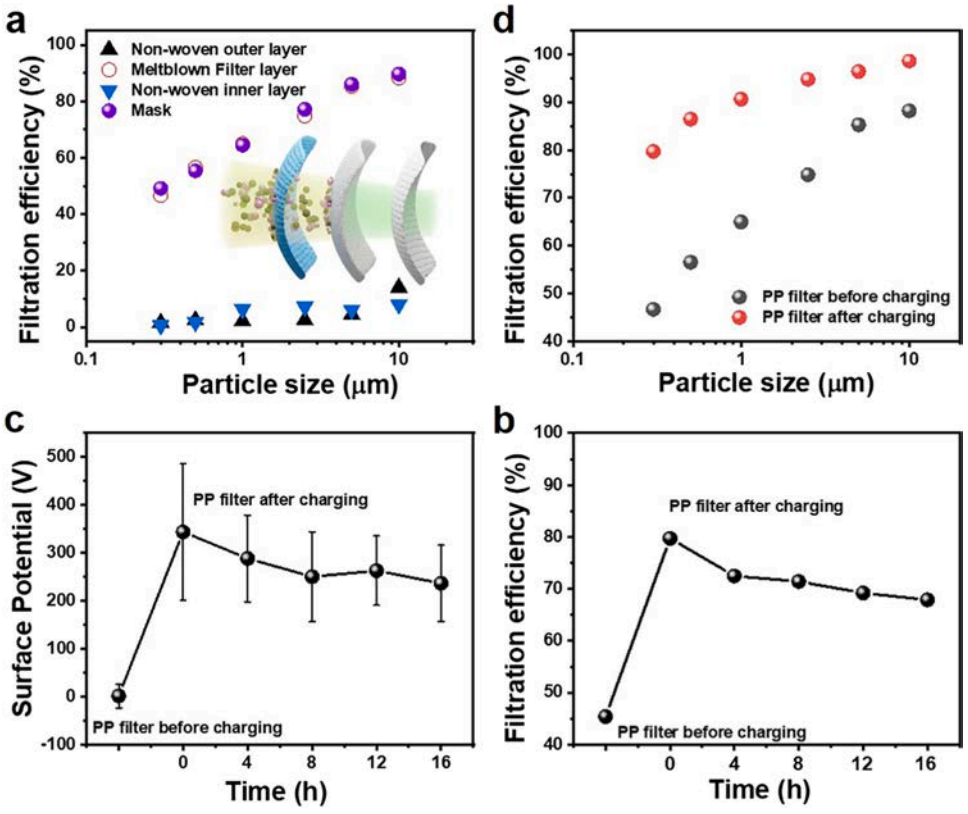

Fig. 1. Particulate matter filtration test and performance of the meltblown PP filter. a) Filtration efficiencies of uncharged disposable surgical mask and different layer of the disposable surgical mask for different-sized PM; The inset is a schematic showing the basic structure of the disposable surgical mask. b) Filtration efficiencies of particle numbers of different-sized PM using the before charging and after charging meltblown PP filter. c) The surface potential of the meltblown PP filter by ESVM-measured that the charged effects are maintained during the period of measurement. Error bar represents the standard deviation of ten replicate measurements. d) 16 h test of the filtration efficiency for $PM_{0.3}$ of the meltblown PP filter.

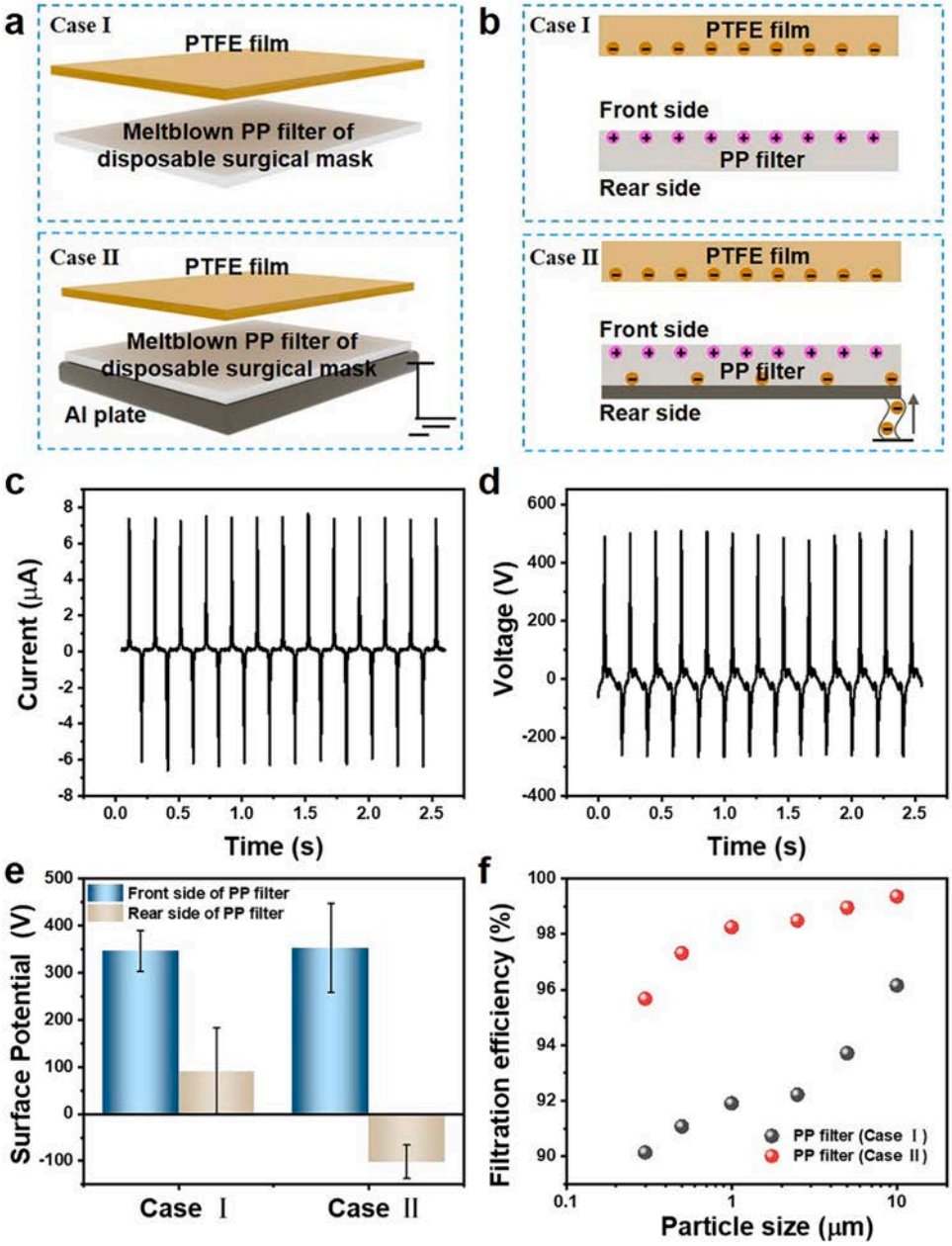

Fig. 2. Meltblown PP filter charging design and working principle a) Schematic illustration of meltblown PP filter and PTFE film as contact layers in sliding mode case I and case II. b) Schematic diagrams that illustrate the process of capturing charged meltblown PP filter case I and case II. c) The short-circuit current of case II. d) The open-circuit voltage of case II. e) The surface potential of the filter front side and rear side. Error bar represents the standard deviation of ten replicate measurements. f) The filtration efficiency of the case I and case II of meltblown PP filter for $PM_{0.3}$–$PM_{10.0}$.

solve this and further enhance the filtration efficiency, the charging scheme is further optimized. The meltblown PP filter is placed upon a grounded Al plate (Fig. 2a, case II), and then rubbed with the PTFE film. In this process, the PTFE and the grounded meltblown PP filter form a single-electrode TENG, the adhesion between the meltblown PP filter and the grounded aluminum plate is guaranteed by the electrostatic adsorption effect. The surface potential of the filter is measured by ESVM.

During the rubbing process, the electrons driven by the displacement current will flow from the ground to the Al plate. In this case, the meltblown PP filter not only plays a role of friction layer but also an electret, and a portion of electrons will dwell in the rear side of the meltblown PP filter to make a bipolar meltblown PP filter, as illustrated in case II of Fig. 2b. The charge distribution in the unipolar charge (charged by conventional method) and bipolar charge (charged by NGCR) are schematically shown in Fig. S2a. According to the charge distribution and solving the corresponding Poisson equation, the electric distribution is obtained (Fig. S2b), and the result shows that the bipolar PP filter has a higher electric field compared with the unipolar PP filter. If the incoming particulates carry net charges, they are then attracted to the meltblown PP fiber surface as passing by due to electrostatic interaction. Even if the particulates are neutral, they are polarized once entering the electric field zone of the meltblown PP filter, and the dipole-dipole interaction can also lead to the deposition of the incoming particulates onto the PP filter [27–29].

Under a driving frequency of 5 Hz, the single-electrode sliding TENG can output a short circuit current of 7.67 μA (Fig. 2c) and an open circuit voltage of 509 V (Fig. 2d). The charge state of the meltblown PP filter is examined by an ESVM (Fig. 2e). The PP filter is flipped when mearing the rear side potential of the PP filter by ESVM. As for the meltblown PP filter charged by rubbing it with a PTFE film, the surface potential of both the front side and rear side of the meltblown PP filter is positive. Compared with the rear side, the surface potential of the front side is higher which indicates the charge in the meltblown PP filter mainly resides on the front side. As for the meltblown PP filter charge by the NGCR, the surface potential of the front side and rear side of the

meltblown PP filter are positive and negative, respectively. This reflects that during the working process of the NGCR, a small portion of electrons has resided into the rear side of the meltblown PP filter. Fig. 2f shows the filtration efficiency of these two cases, the meltblown PP filter charged with the NGCR has a higher filtration efficiency compared with the meltblown PP the above results reveal that making the meltblown PP filter electrified with NGCR can greatly improve its filtration efficiency for micro/nanoparticles. For the practical application of this technical scheme on disposable surgical masks, it should not induce the morphological and structural degeneration of meltblown PP filter, otherwise, the meltblown PP filter will be worn down and can't afford long-term high efficiency filtration function. So, wear resistance of the meltblown PP filter after the rubbing process is characterized. The morphologies before and after rubbing process are characterized by the scanning electron microscope (SEM). As shown in Fig. 3a–c, after 300 and 500 times of rubbing, no notable morphological changes in meltblown PP filter are found. The pressure drop of the meltblown PP filter at different friction times are nearly the same (Fig. S3). The differences between the strain-stress curves of the meltblown PP filter before and after frictions is very small, indicating that the friction process has little damage to the meltblown PP filter structure (Fig. S4).

After rubbing 500 times, the porosity of the meltblown PP filter changes from 5.7% to 4.9% (Fig. S5), which indicates the structure of the meltblown PP filter is stable against rubbing. Fourier transforms infrared (FTIR) spectra (Fig. 3d) is used to characterize the structure of the meltblown PP filter. In the FTIR spectra, the characteristic vibration peak of $–CF_2–$ are not found in PP filter with different friction times, which indicate there doesn't exist material transfer between the PP and PTFE during the rubbing process. Therefore, making the meltblown PP filter electrified by NGCR technology is effective and suitable for practical application.

2.3. Filtration performance enhancement of meltblown PP filter after using the NGCR technology

Next, the friction times of the single-electrode TENG are optimized to obtain a higher filtration efficiency. As shown in Fig. 4a, with the increase of friction times, the surface potential of the PP filter increases rapidly at first and then is gradually toward a saturated value. the rear side surface potential of the meltblown PP filter is showed in Fig. S6a. So, 500 times of friction is enough to electrify the PP filter. As shown in Fig. 4b, after the meltblown PP filter is electrified, even after 12 h, the surface potential of the meltblown PP filter can still be maintained at a relatively large value (219 V), the rear side surface potential of the meltblown PP filter is −140 V (Fig. S6b). During the charging process, a portion of charges will enter the interior of the material. Even for the surface charge, a part of the charge is trapped in the deep defects of the electret [30–32]. As a large activation energy is needed to release this kind of charges, the surface potential of the electret can maintain for a long time. The activation of the trapped charge can be reflected by the location of current peak in the thermally stimulated discharge (TSD) spectrum, higher temperature corresponds to larger activation energy [33–35]. As for the charged PP filter, the current peak at 148 °C (Fig. S7) corresponds to deep defects with a large activation energy, which ensures the long-term high filtration efficiency of the charged meltblown PP filter (Fig. S8). Fig. 4c compares the filtration efficiency of the meltblown PP filter layer of disposable surgical mask for PMs with different sizes before and after the charging process with our optimized NGCR scheme. After the meltblown PP filter layer is charged through NGCR technological scheme, the filtration efficiency of the meltblown PP filter for all the PMs is greatly enhanced, where the filtration efficiencies for the $PM_{0.3}$, $PM_{0.5}$, $PM_{1.0}$, $PM_{2.5}$, $PM_{5.0}$, and $PM_{10.0}$ are increased from 46.7%, 56.5%, 64.9%, 74.8%, 85.3% and 88.2% to

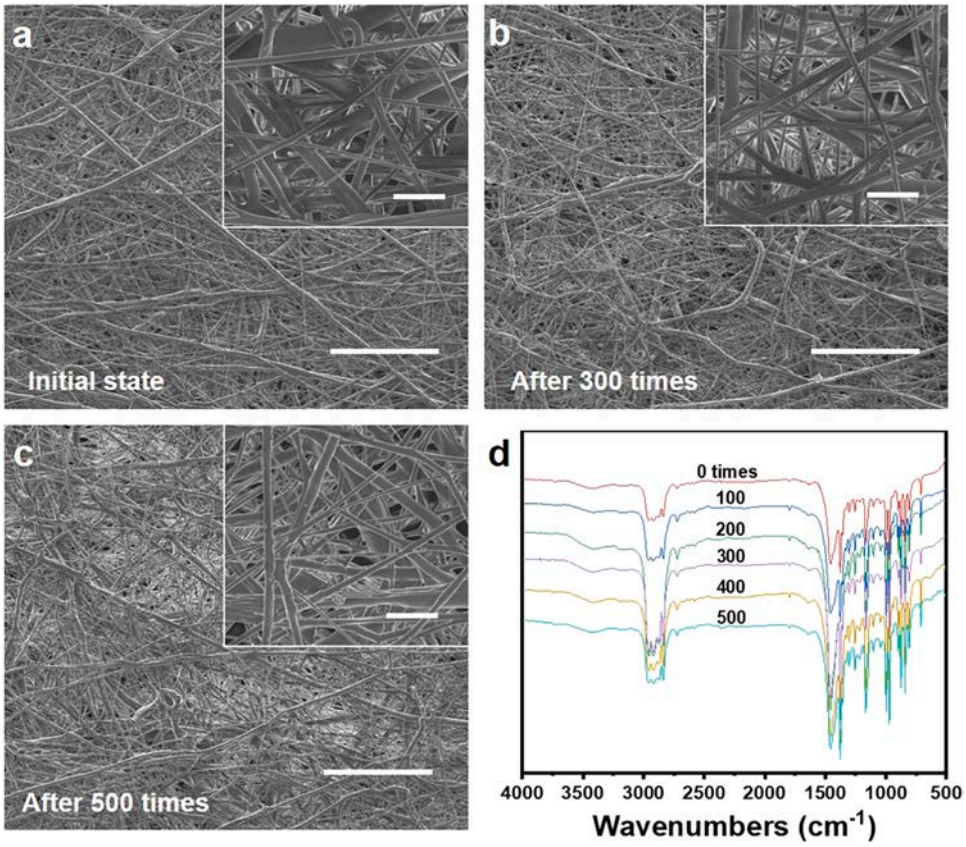

Fig. 3. Characterization of wear resistance. a), b), c) Microscopic morphologies of the meltblown PP filter in top-down viewed SEM images at different friction times (scale bar: 200 μm); the inset is a higher resolution SEM image of meltblown PP filter (scale bar: 20 μm). d) FTIR spectra of meltblown PP filter of different friction times.

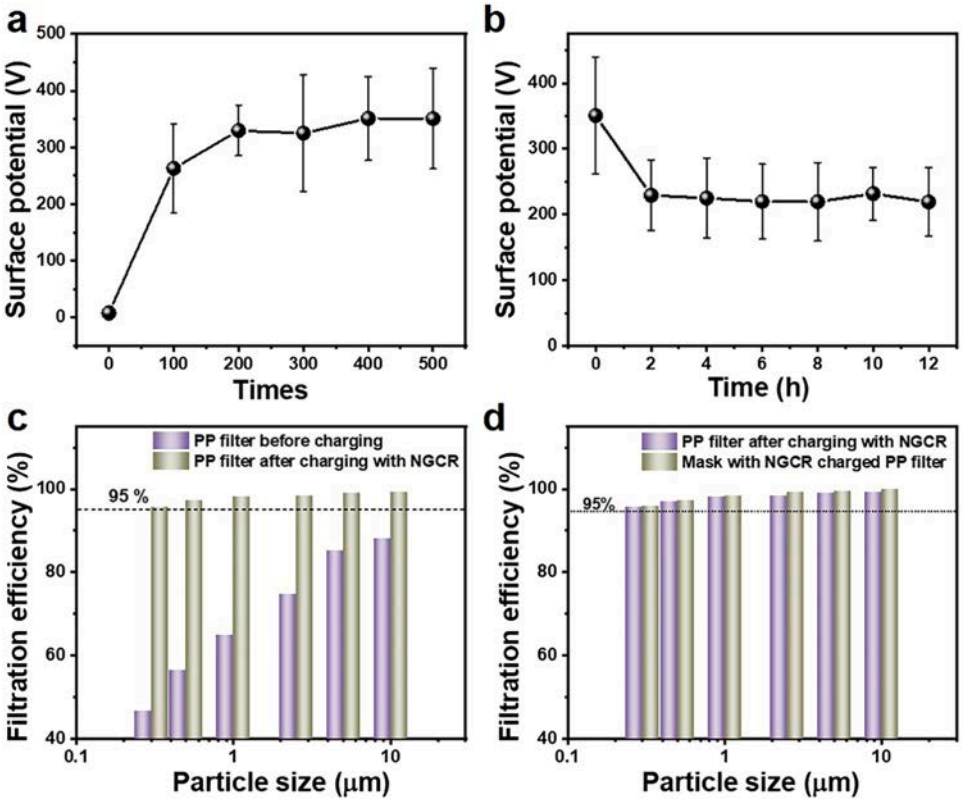

Fig. 4. Performance enhancement of meltblown PP filter after applying the NGCR technology. a) The surface potential of the meltblown PP filter front side with different friction times with NGCR technology. b) 12 h test of the surface potential of the meltblown PP filter. Error bar represents the standard deviation of ten replicate measurements. c) The filtration efficiency of the before charging and after charging meltblown PP filter with NGCR technology. d) The filtration efficiency of the charged meltblown PP filter and disposable surgical mask with NGCR technology charged meltblown PP filter.

95.7%, 97.3%, 98.3%, 98.5%, 99.0% and 99.4%, respectively. It is clear that the smaller particle sizes, the greater enhancement in filtration efficiency. For $PM_{0.3}$, the filtration efficiency of the charged PP filter is 2.05 times as large as the filtration efficiency of the uncharged PP filter. As shown in Fig. 4d, the filtration efficiency of the electrified meltblown PP filter with the NGCR is comparable to the filtration efficiency of the disposable surgical mask containing electrified meltblown PP filter with the NGCR. As shows in Fig. S9, under high relative humidity, the charged meltblown PP filter of the mask can still maintain a high filtration efficiency. The filtration efficiency of the disposable surgical mask is determined by the charged meltblown PP filter.

2.4. Evaluation and selection of the optimal decontamination method

In practical applications, besides the filtration efficiency, the decontamination of disposable surgical masks is also important. Now, there exist various decontamination methods including the typical 75% alcohol immersing, 80 °C water bathing, and 80 °C dry heating. For these 3 typical decontamination methods, we tested their effectiveness, where the structural change and lived bacterial colony are severed as indicators. The less the structural change of the disposable surgical masks, the fewer the lived bacterial colony, the better the effectiveness of the decontamination method. As shown in Fig. 5a–d, all of the three decontamination methods can completely inactive the Staphylococcus aureus (*S. aureus*). The stability of surface property and structure is verified by hydrophobic testing, if the contact angle of the droplet deposited on the meltblown PP filter changed notably, there would also a large change of the meltblown PP filter's structure or surface property. The water contact angle of the pristine meltblown PP filter is 136° (Fig. 5e). After the 30 min decontamination treatment with 75% alcohol immersing, 80 °C water bathing, and 80 °C dry heating, respectively, the water contact angle of the pristine meltblown PP filter is 123° (Fig. 5f), 119° (Fig. 5g), and 127° (Fig. 5h). But according to Fig. S10 SEM images, there is no big difference in the morphology after different methods of decontamination. Further, the front side surface potential and filtration efficiency of meltblown PP filter before charging, after charging and after decontamination, are compared (Fig. 5i and j). The rear side surface potential is showed in Fig. S11. The surface potential of meltblown PP filters being disinfected with 75% alcohol immersing or 80 °C water bathing is almost zero, and the filtration efficiency toward $PM_{0.3}$ almost returns to the initial value. In contrast, the front side surface potential of meltblown PP filter disinfected with 80 °C dry heating is about 80 V (the rear side surface potential −24 V), and its filtration efficiency of $PM_{0.3}$ is 80% which is higher than the original value of 34.2%. Based on the above analysis, it can be seen that the 80 °C dry heating decontamination method is most effective.

2.5. Developing regeneration procedure for multiple uses of the disposable surgical mask

Without destroying the overall structure of disposable surgical mask (as show in Figs. S12 and S13), we took the 80 °C dry heating decontamination and the filter charge replenishment by NGCR as a regeneration procedure for the disposable surgical masks. After electrifying the initially uncharged meltblown PP filter by the NGCR technology, the $PM_{0.3}$ filtration efficiency increases from 34.3% to 95.1% as shown in Fig. 6a. A moisture treatment is used to simulate wearing the mask for 4 h as shown in Fig. S14. After the moisture treatment and 80 °C dry heating decontamination of disposable surgical masks, the filtration efficiency declined to 79.8%. By again using NGCR to replenish the meltblown PP filter charge, the $PM_{0.3}$ filtration efficiency returned to 95%. Fig. 6a shows the filtration efficiency of the meltblown PP filter after moisture treatment, decontamination, and charge replenishment. After ten such cycles, the filter's filtration efficiency can remain about 95%. As shown in Fig. S15, characterize the morphology and structure of the PP melt-blown filter by the SEM, which indicates the structure of the meltblown PP filter is stable after the cyclic tests.

As for the disposable surgical mask with pristine charged meltblown PP filter, with the increased cycles of moisture treatment and subsequent decontamination, its filtration efficiency gradually decreases as shown

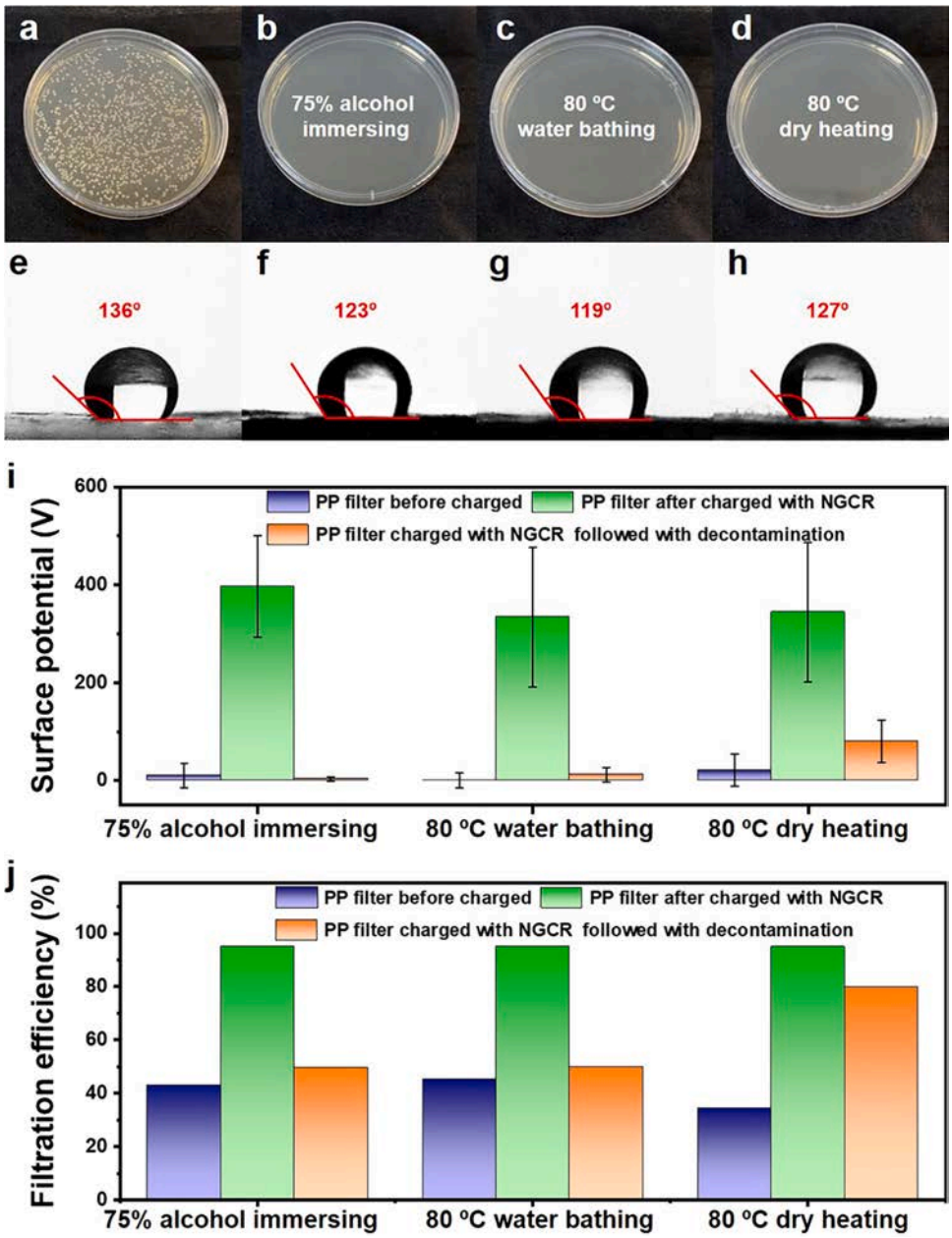

Fig. 5. Summary of the decontamination method and effect on meltblown PP filter performance. a) Photographs of *S. aureus* colonies on agar plates after co-culturing for 24 h a) control group; b) 75% alcohol immersing; c) 80 °C water bathing; d) 80 °C dry heating; e)–h) Apparent water contact angles of meltblown PP filter with respect to various decontamination methods. i) The front side surface potential of the meltblown PP filter for the before charging, after charging and after different decontamination methods. j) $PM_{0.3}$ filtration efficiency of the meltblown PP filter for the before charging, after charging and after different decontamination methods. Error bar represents the standard deviation of ten replicate measurements.

in the inset of Fig. 6b. After four such cycles, the filtration efficiency of $PM_{0.3}$ has reduced from the original value of 99.2–85.6%. After electrifying the initially charged meltblown PP filter by the NGCR technology, the filter's filtration efficiency can be improved to 95.3%. After ten cycles of the simulated wearing process of 4 h and regeneration procedures, the $PM_{0.3}$ filtration efficiency of the meltblown PP filter can remain beyond 95%, which demonstrating its excellent reproducibility. So, the 80 °C dry heating method and the meltblown PP filter charge replenishment by NGCR can make up an effective regeneration procedure for disposable surgical masks to prolong their lifetime.

3. Discussion

In summary, we demonstrate an effective scheme to make the disposable surgical masks reusable without changing their structure and production process. The gradually dissipated charges on the filter layer after long-term use are replenished using a NGCR technology. Without changing the structure of the existing 3-layer disposable surgical masks, the filtration efficiency of the bipolar charged filter towards $PM_{2.5}$ increases from the original value 74.8–98.5%. This enhancement can be ascribed to the higher electric filed inside the bipolar charged filter. Moreover, among various decontamination methods for disposable surgical masks, we find that the 80 °C dry heating method is most promising as it doesn't bring out changes in mask's structure and exhibits relatively high charge stability during the decontamination process. So, the 80 °C dry heating method and the filter charge replenishment with NGCR can make up regeneration procedure for the disposable surgical masks. Even after ten cycles of simulated 4 h wearing process and such regeneration procedures, the filtration efficiency of the disposable surgical masks towards $PM_{0.3}$ is still about 95%.

4. Methods

4.1. Fabrication of TENG

Firstly, the PTFE film was washed in the ethanol and DI water. PTFE

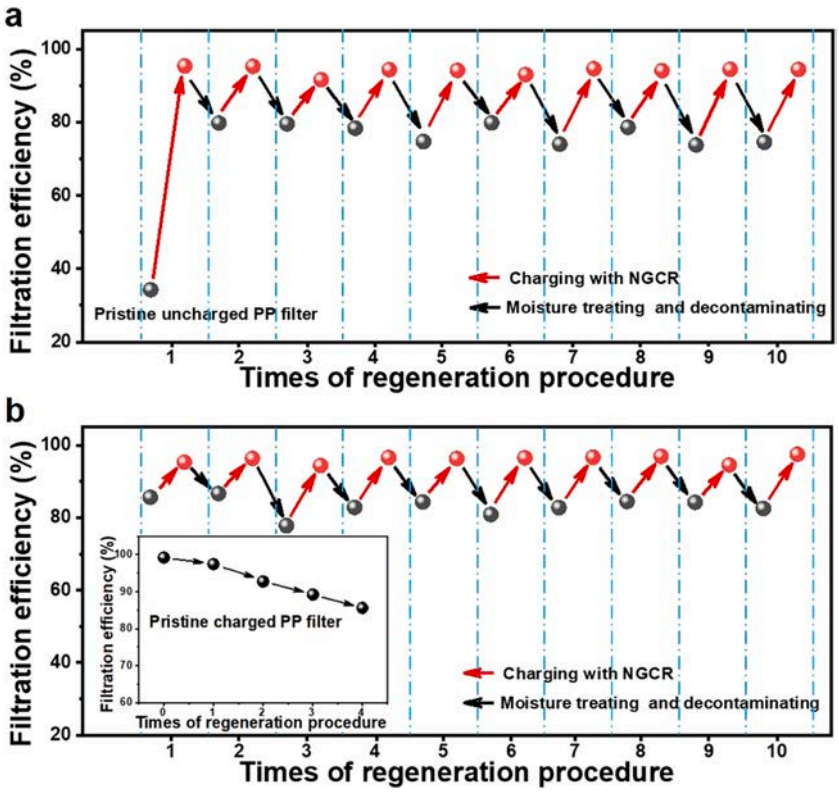

Fig. 6. Regeneration test and filtration performance. a) Filtration efficiency of the pristine uncharged meltblown PP filter regenerated for 1–10 times. b) Filtration efficiency of the pristine charged meltblown PP filter regenerated for 1–10 times. The inset is the filtration efficiency of the pristine charged meltblown PP filter for $PM_{0.3}$ after simulated breath moisture test for 0–4 times.

film and meltblown PP filter of disposable surgical masks were tailored into a disc with a radius of 2.5 cm as frictional layers. Secondly, the meltblown PP filter is placed on a grounded aluminum (Al) plate. Finally, cooper wire was led out from the Al plate for electrical measurement.

4.2. Filtration efficiency measurement

A handheld particle counter (DT-9881M, CEM, China) was used to detect the PM particle number concentration before and after filtration. The filtration efficiency was calculated by comparing the number concentration before and after filtration.

4.3. Decontamination experiment

Firstly, *streptococcus aureus* suspension (0.1 mL, 10^5 CFU/mL) was added on the surface of four meltblown PP filters (1 cm × 1 cm), respectively. Secondly, three of them were treated with 75% alcohol immersing, 80 °C water bathing, and 80 °C dry heating for 30 min, respectively. The remaining untreated one was used as the control group. Thirdly, the four samples were washed with sterile water, and the supernatant contains bacterial were collected, respectively. Finally, the collected 0.1 mL of the bacterial mixture were added into four nutrient agar plates directly. The plates were incubated at 35 °C for 24 h. After that, the bacterial colony was counted. A schematic about this process was shown in Fig. S16.

4.4. Simulated breath moisture test

The water produced by human breathing per day is about 350–400 mL, which equals to a flow rate about 0.24–0.27 mL/min [36]. The area of the unfolded disposable surgical mask is 15 × 14 cm^2. The amount of water passing through the mask per area for 4 h is about 0.27–0.31/cm^2. Firstly, the spray rate of the compressed atomizer with an outlet radius of 1.8 cm was adjusted to 0.25 mL/min to match the flow rate of the water produced by human respiration. Secondly, the unfolded disposable surgical mask was tailored into a disc with a radius of 2.5 cm. Finally, the disc is placed on the compressed atomizer for 12 min. In this process the amount of water passing the disc is 0.29 mL/cm^2, which is comparable to the value (0.27–0.31 mL/cm^2) of wearing the disposable surgical mask for 4 h (2).

4.5. Characterization of the device

The short-circuit current was measured by a current preamplifier (SR570, Stanford Research Systems, USA). The surface potential of the meltblown PP was measured by an electrostatic voltmeter (Model 279, Monroe Electronics Company, USA). The morphology of meltblown PP filters was characterized by a scanning electron microscope (SEM, HITACHI S4800). The absorbance peaks of the FTIR spectrum were measured by the FTIR spectrometer (NEVUS 670, Nicolet).

Author contributions

Y.Q. put forward the idea and the project. Y.Q. and Q.X. designed the experiment. R.C.Z. did the experiments. R.C.Z., Q.X. and Y.Q. wrote the manuscript. All authors analyzed the results and have given approval to the final version of the manuscript. R.C.Z. and Q.X. contributed equally to this work.

CRediT authorship contribution statement

Ruichao Zhang: Conceptualization, Writing - review & editing, Methodology, Visualization, Investigation. **Qi Xu:** Conceptualization, Writing - review & editing, Methodology, Visualization, Formal analysis. **Suo Bai:** Methodology, Visualization, Investigation. **Jun Hai:**

Investigation. **Li Cheng:** Investigation. **Yong Qin:** Conceptualization, Writing - review & editing, Supervision, Project administration.

Declaration of Competing Interest

The authors declare that they have no known competing financial interests or personal relationships that could have appeared to influence the work reported in this paper.

Acknowledgments

We sincerely acknowledge the support from the Joint Fund of Equipment Pre-research and Ministry of Education (No. 6141A02022518), the National Program for Support of Topnotch Young Professionals, the Fundamental Research Funds for the Central Universities (No. lzujbky-2020-sp08). We thank Qiangqiang Zhang, Guoqiang Xu, Weihua Han, Qi Zhang, Kun Yu and Zelin Lei for the nice discussions.

Appendix A. Supplementary material

Supplementary data associated with this article can be found in the online version at doi:10.1016/j.nanoen.2020.105434.

References

[1] L. Morawska, J. Cao, Airborne transmission of SARS-CoV-2: the world should face the reality, Environ. Int. 139 (2020), 105730.
[2] J.L. Santarpia, D.N. Rivera, V. Herrera, M.J. Morwitzer, H. Creager, G.W. Santarpia, K.K. Crown, D. Brett-Major, E. Schnaubelt, M.J. Broadhurst, J.V. Lawler, S.P. Reid, J.J. Lowe, Transmission Potential of SARS-CoV-2 in Viral Shedding Observed at the University of Nebraska Medical Center, medRxiv, 2020. Available from: ⟨https://doi.org/10.1101/2020.03.23.20039446⟩.
[3] J. Wang, G. Du, COVID-19 may transmit through aerosol, Ir. J. Med. Sci. (2020). Available from: ⟨https://link.springer.com/article/10.1007/s11845-020-02218-2⟩.
[4] E.Y.C. Shiu, N.H.L. Leung, B.J. Cowling, Controversy around airborne versus droplet transmission of respiratory viruses: Implication for infection prevention, Curr. Opin. Infect. Dis. 32 (2019) 372–379.
[5] A.C. Lai, C.K. Poon, A.C. Cheung, Effectiveness of facemasks to reduce exposure hazards for airborne infections among general populations, J. R. Soc. Interface 9 (2012) 938–948.
[6] N.H.L. Leung, D.K.W. Chu, E.Y.C. Shiu, K.-H. Chan, J.J. McDevitt, B.J.P. Hau, H.-L. Yen, Y. Li, D.K.M. Ip, J.S.M. Peiris, W.-H. Seto, G.M. Leung, D.K. Milton, B. J. Cowling, Respiratory virus shedding in exhaled breath and efficacy of face masks, Nat. Med. 26 (2020) 676–680.
[7] R.J. Thomas, Particle size and pathogenicity in the respiratory tract, Virulence 4 (2013) 847–858.
[8] H. Souzandeh, L. Scudiero, Y. Wang, W.-H. Zhong, A disposable multi-functional air filter: paper towel/protein nanofibers with gradient porous structures for capturing pollutants of broad species and sizes, ACS Sustain. Chem. Eng. 5 (2017) 6209–6217.
[9] S. Zhang, H. Liu, X. Yin, J. Yu, B. Ding, Anti-deformed polyacrylonitrile/polysulfone composite membrane with binary structures for effective air filtration, ACS Appl. Mater. Interfaces 8 (2016) 8086–8095.
[10] M. Lalagiri, G. Bhat, V. Singh, S. Parameswaran, R.J. Kendall, S. Ramkumar, Filtration efficiency of submicrometer filters, Ind. Eng. Chem. Res. 52 (2013) 16513–16518.
[11] Centers for Disease Control and Prevention (CDC). N95 Respirators and Surgical Masks, 2009. Available from: ⟨https://blogs.cdc.gov/niosh-science-blog/2009/10/14/n95/⟩.
[12] T.-M. Chen, C.-J. Tsai, S.-Y. Yan, S.-N. Li, An efficient wet electrostatic precipitator for removing nanoparticles, submicron and micron-sized particles, Sep. Purif. Technol. 136 (2014) 27–35.
[13] K.Y. Liu, J.Y. Rau, M.Y. Wey, Collection of SiO_2, Al_2O_3 and Fe_2O_3 particles using a gas-solid fluidized bed filter, J. Hazard. Mater. 171 (2009) 102–110.
[14] X. Zhao, Y. Li, T. Hua, P. Jiang, X. Yin, J. Yu, B. Ding, Low-resistance dual-purpose air filter releasing negative ions and effectively capturing $PM_{2.5}$, ACS Appl. Mater. Interfaces 9 (2017) 12054–12063.
[15] S. Jung, J. An, H. Na, J. Kim, Surface energy of filtration media influencing the filtration performance against solid particles, oily aerosol, and bacterial aerosol, Polymers 11 (2019) 935.
[16] J. Lee, J. Kim, Material properties influencing the charge decay of electret filters and their impact on filtration performance, Polymers 12 (2020) 721.
[17] G.H. Zhang, Q.H. Zhu, L. Zhang, F. Yong, Z. Zhang, S.L. Wang, Y. Wang, L. He, G. H. Tao, High-performance particulate matter including nanoscale particle removal by a self-powered air filter, Nat. Commun. 11 (2020) 1653.
[18] K. Hu, R. Xiong, H. Guo, R. Ma, S. Zhang, Z.L. Wang, V.V. Tsukruk, Self-powered electronic skin with biotactile selectivity, Adv. Mater. 28 (2016) 3549–3556.
[19] C. Wu, A.C. Wang, W. Ding, H. Guo, Z.L. Wang, Triboelectric nanogenerator: a foundation of the energy for the new era, Adv. Energy Mater. 9 (2018), 1802906.
[20] Q. Xu, L. Cheng, L.X. Meng, Z. Wang, S. Bai, X. Tian, X. Jia, Y. Qin, Flexible self-powered ZnO film UV sensor with a high response, ACS Appl. Mater. Interfaces 11 (2019) 26127–26133.
[21] X. Cao, Y. Jie, N. Wang, Z.L. Wang, Triboelectric nanogenerators driven self-powered electrochemical processes for energy and environmental science, Adv. Energy Mater. 6 (2016), 1600665.
[22] Y. Jie, Q. Jiang, Y. Zhang, N. Wang, X. Cao, A structural bionic design: from electric organs to systematic triboelectric generators, Nano Energy 27 (2016) 554–560.
[23] Y. Bai, C.B. Han, C. He, G.Q. Gu, J.H. Nie, J.J. Shao, T.X. Xiao, C.R. Deng, Z. L. Wang, Washable multilayer triboelectric air filter for efficient particulate matter PM2.5 removal, Adv. Funct. Mater. 28 (2018), 1706680.
[24] S. Chen, C. Gao, W. Tang, H. Zhu, Y. Han, Q. Jiang, T. Li, X. Cao, Self-powered cleaning of air pollution by wind driven triboelectric nanogenerator, Nano Energy 14 (2015) 217–225.
[25] Y. Feng, L. Ling, J. Nie, K. Han, X. Chen, Z. Bian, H. Li, Z.L. Wang, Self-powered electrostatic filter with enhanced photocatalytic degradation of formaldehyde based on built-in triboelectric nanogenerators, ACS Nano 11 (2017) 12411–12418.
[26] P.A. Smith, G.C. East, R.C. Brown, D. Wake, Generation of triboelectric charge in textile fibre mixtures, and their use as air filters, J. Electrost. 21 (1988) 81–98.
[27] G. Liu, J. Nie, C. Han, T. Jiang, Z. Yang, Y. Pang, L. Xu, T. Guo, T. Bu, C. Zhang, Z. L. Wang, Self-powered electrostatic adsorption face mask based on a triboelectric nanogenerator, ACS Appl. Mater. Interfaces 10 (2018) 7126–7133.
[28] K.S. Han, S. Lee, M. Kim, P. Park, M.H. Lee, J. Nah, Electrically activated ultrathin PVDF-TrFE air filter for high-efficiency PM1.0 filtration, Adv. Funct. Mater. 29 (2019), 1903633.
[29] Y. Cheng, C. Wang, J. Zhong, S. Lin, Y. Xiao, Q. Zhong, H. Jiang, N. Wu, W. Li, S. Chen, B. Wang, Y. Zhang, J. Zhou, Electrospun polyetherimide electret nonwoven for bi-functional smart face mask, Nano Energy 34 (2017) 562–569.
[30] J.V. Turnhout, Thermally stimulated discharge of polymer electrets, Polym. J. 2 (1971) 173–191.
[31] N.Y. Cui, L. Gu, Y.M. Lei, J.M. Liu, Y. Qin, X.H. Ma, Y. Hao, Z.L. Wang, Dynamic behavior of the triboelectric charges and structural optimization of the friction layer for a triboelectric nanogenerator, ACS Nano 10 (2016) 6131–6138.
[32] J. Wang, D. Rychkov, Q.D. Nguyen, R. Gerhard, The influence of orthophosphoric-acid surface modification on charge-storage enhancement in polypropylene electrets, J. Appl. Phys. 128 (2020), 034102.
[33] A.G. Kravtsova, H. Brünigb, S.F. Zhandarovb, Analysis of the polarization state of melt-spun polypropylene fibers, J. Mater. Process. Technol. 124 (2002) 160–165.
[34] J. Hillenbrand, N. Behrendt, V. Altstädt, H.W. Schmidt, G.M. Sessler, Electret properties of biaxially stretched polypropylene films containing various additives, J. Phys. D Appl. Phys. 39 (2006) 535–540.
[35] D. Min, C. Yan, R. Mi, C. Ma, Y. Huang, S. Li, Q. Wu, Z. Xing, Carrier transport and molecular displacement modulated dc electrical breakdown of polypropylene nanocomposites, Polymers (Basel) 10 (2018) 1207.
[36] A.C. Guyton, J.E. Hall, Textbook of Medical Physiology, Elsevier Inc., Philadelphia, 2000.